Dynamic polarization potential for ^{6}He+p due to breakup

R. S. Mackintosh*
Department of Physics and Astronomy, The Open University, Milton Keynes, MK7 6AA, United Kingdom

K. Rusek
Department of Nuclear Reactions, The Andrzej Sołtan Institute for Nuclear Studies, Hoża 69, 00-681 Warsaw, Poland

(Received 13 March 2002; revised manuscript received 18 October 2002; published 20 March 2003)

We study the local dynamic polarization potential (DPP) component of the ^{6}He+p interaction, determining that part which is due to breakup processes. Results are presented for c.m. energies of 21.57 and 35.06 MeV. The DPP is found by subjecting the elastic scattering S matrix from continuum-discretized coupled-channels calculations to S matrix→potential inversion. The iterative-perturbative inversion method is employed, and the method is shown to give reliable potentials down to projectile-target separation close to zero, a necessary requirement for this case. The contributions of different continuum states are compared, and the way they interact to give the overall DPP is studied. The DPP is found to be very different from that determined using the weighted trivially equivalent approximate method.

DOI: 10.1103/PhysRevC.67.034607 PACS number(s): 24.10.−i, 25.10.+s, 25.60.−t, 25.40.Cm

I. INTRODUCTION

A full understanding of the interaction between nucleons and nuclei or between pairs of nuclei requires an understanding of the contribution of excitation and transfer processes which occur as nuclei interact. In this paper we demonstrate, in the context of $p+^6$He elastic scattering, how the use of inversion techniques should enable a systematic investigation of these contributions.

The contributions of breakup, excitation, and transfer processes are conventionally represented by the dynamic polarization potential (DPP) and there are many papers which claim to determine this and also exploit it. We shall show that there are shortcomings in methods sometimes used to establish DPPs. We present a method that is able to give consistent and reliable results and is straightforward enough to become a routine adjunct to reaction calculations.

The calculations presented here are conceptually straightforward: the elastic channel S matrix, generated by continuum-discretized coupled-channel (CDCC) calculations, including breakup processes, is subjected to $S\rightarrow V(r)$ inversion. The bare potential of the CDCC calculations is then subtracted from $V(r)$ and the remainder is identified as the DPP. The inversion is carried out using the iterative-perturbative (IP) method [1–3] which can give very reliable potentials, including spin-orbit potentials for the spin-half case, for all relevant radii. The model used for ^{6}He, while simplified, is rich enough to provide a number of insights and achieve the specific aims of this study listed below.

Specific aims are as follows.

(1) To show that the IP inversion method can reliably determine the DPP in the present unfavorable case and establish the necessary ''inversion parameters'' (these latter must be chosen carefully for successful inversion in the case of a spin 1/2 projectile and a limited number of contributing partial waves).

(2) To establish the breakup contribution to the DPP for a nucleon interacting with the halo nucleus ^{6}He according to a specific breakup model.

(3) In the context of this model, to establish generic features of the DPP and its dependence upon such things as the l transfer and other characteristics of the specific reaction channels. In particular, to study its radial shape and verify or otherwise the common phenomenological representation of the DPP as a uniform renormalization of a folding model potential.

(4) To evaluate the weighted trivially equivalent (WTE) method for determining the DPP.

Many other reactions beside the breakup contributions contribute to the elastic scattering of ^{6}He from protons. A full calculation including them all, respecting nonorthogonality terms, exchange processes, finite range transfer, etc., is a formidable task, and it could not be an aim of this work to determine the complete DPP.

The plan of this paper is as follows. Section II reviews the general problems of identifying and determining the DPP. Section III briefly reviews relevant aspects of $p+^6$He scattering. Section IV presents the model for ^{6}He breakup. Section V concerns the application of IP inversion to the specific case of $p+^6$He scattering. Section VI presents the results concerning the breakup contribution to the DPP for $p+^6$He elastic scattering and Sec. VII summarizes the conclusions.

II. THE DYNAMIC POLARIZATION POTENTIAL

A. Conceptual difficulties

The nucleus-nucleus potential is often thought of as composed of a folding model potential and a dynamic polarization potential. Behind this idea stands Feshbach's theory [4] according to which the effective potential in the elastic channel is

$$\mathcal{V}^P = P\left[V + VQ\frac{1}{E+i\epsilon-QHQ}QV\right]P, \qquad (1)$$

where V is the projectile-target interaction. Projection operator P projects onto internal nuclear states for the elastic chan-

*Electronic address: r.mackintosh@open.ac.uk

nel, with $P+Q=1$. The second term is the contribution to the effective potential, $\mathcal{V}$, of virtual excitations of the interacting nuclei and is known as the dynamic polarization potential. In fact, there are serious difficulties of calculation and also interpretation: (1) If PVP is represented by a folding model potential, as is often the case, then there is an indefinite degree of double counting since theoretical folding models include particle hole excitations. (2) Reaction channels make a major contribution to $\mathcal{V}$, but nonorthogonality between different channels poses a severe challenge. (3) The requirement of antisymmetrization is very difficult to implement. (4) There are vast numbers of states that should in principle be included together with coupling between each pair. (5) The second term is both nonlocal and L dependent.

The difficulties are exemplified by proton scattering from nuclei where a very substantial DPP arising from coupling to pickup channels has been established [5]. Yet folding model analyses appear not to require this correction. The states contributing to the DPP are not orthogonal to the particle-hole contribution to the folding model potential which cannot use bare nucleon-nucleon interactions. It therefore appears that the effect of coupled channels is included in the folding model to some unknown extent and only in an average way. The folding model being a local density model cannot represent L-dependent effects. But there is evidence both that the DPP calculated directly from CRC calculations does represent an L-dependent effect and that precision fits to elastic scattering data do suggest L dependence (distinct from parity dependence).

B. Why the DPP is required

In spite of serious conceptual difficulties, the concept of a DPP is widely used and many papers claim to determine it. To cite a single example, the detailed analysis of the ^{6}Li folding model by Khoa *et al.* [6] makes essential use of the DPP due to breakup of the ^{6}Li projectile. While the DPP in the far surface region is probably established (solving anomalies in the ^{6}Li potential), the DPP at somewhat smaller radii is not so well established, and in fact there are differences between that used by Khoa *et al.* and that established by inversion methods [1,2]. It is quite clear that the rigorous evaluation of folding models demands a more detailed systematic knowledge of the DPP. For the case of composite projectiles, it has been known for many years [7] that collective target states lead to surface attraction or repulsion and the DPP consequently affects the extraction of nuclear size information from elastic scattering.

It is important to understand the contribution of specific direct processes since these are not fully represented by current folding models based on a local density approximation. Such processes explain, for example, departures from the global behavior of internuclear potentials, and could reveal new features of elastic scattering of weakly bound nuclei. Certainly, a fuller understanding of elastic scattering than presently exists is a prerequisite for the rigorous extraction of spectroscopic information from direct reactions. It might be possible to establish an optical model equivalent of the Strutinsky model in which the DPP is divided into smooth and fluctuating components with the smooth part represented by the folding model.

C. Determining the DPP

Most attempts to determine the DPP fall into three categories.

Phenomenological. Fit data with $V_{\rm fold}+V_{\rm correction}$ and identify the correction as the DPP. This assumes that $V_{\rm fold}$ is appropriate and does not contain any part of the DPP, although in fact it must contain some part of the DPP. This method has the uncertainty of optical model searching together with the uncertainty associated with the poorly defined boundary between folding potential and DPP. It does not permit the identification of specific components of the DPP

Theoretical method 1, explicit calculation of Green's functions. This is very hard when, as is often necessary, interchannel coupling makes this a complex iterative problem. For an example of a calculation in which interchannel coupling is omitted, leading to a simple sum of terms, see Coulter and Satchler [8].

Theoretical method 2, coupled channel plus inversion. Three steps: (i) Coupled channel gives S_{lj} elastic; (ii) invert $S_{lj}\rightarrow V$ to get local representation of $\mathcal{V}^P$; (iii) subtract the bare V of the CC calculation, $\mathcal{V}^\pi$ as defined in Eq. (2).

A further problem with the first theoretical method is that it yields a nonlocal and L-dependent potential that cannot readily be compared with phenomenological potentials. Method 2 gives a local potential directly that is a local equivalent of a nonlocal and L-dependent potential. Many DPPs calculated this way involve approximate inversions, such as the weighted trivial equivalent (WTE) method or eikonal methods. This paper shall compare WTE results with exact inversion in for $p+^6$He elastic scattering.

D. Formal theory of contribution to DPP of specific channels

We review the formal basis of the DPP calculations. Assume a set of specific states of interest are coupled to the elastic channel and correspond (in Feshbach sense) to projection operator p and that all the other states correspond to projection operator q.

With the elastic channel represented by projection operator P, we have $P+p+q=1$ so that the ''usual'' $Q=p+q$, etc. The space of the coupled channel calculations is defined by projection operator $\pi=P+p$.

We regard the contributions of q states as being smoothly varying, analogous to macroscopic term in Strutinsky model; this might even be folding model space. In the same way, the contributions of p space lead to the specific effects of particular strongly coupled, low excitation channels (cf. shell correction term in Strutinsky model).

Define

$$\mathcal{V}^\pi=\pi\left[V+Vq\frac{1}{E+i\epsilon-qHq}qV\right]\pi, \tag{2}$$

the appropriate interaction for use in a π-space calculation. The collective contribution of p-space states $\Delta\mathcal{V}=\mathcal{V}^P-\mathcal{V}^\pi$ can be shown [7] to be

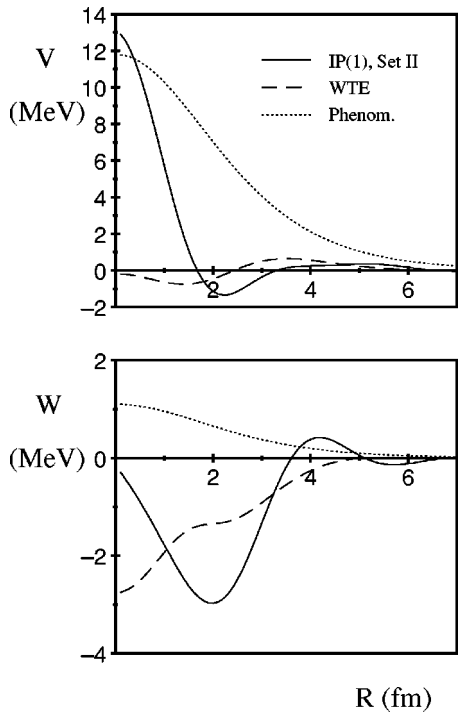

FIG. 1. Real and imaginary parts of three polarization potentials for ^{6}He+p elastic scattering. Two of them IP and WTE were obtained from CDCC analysis of elastic scattering data at $E_{\text{c.m.}}=21.57$ MeV in this work and in Ref. [9], respectively. The third, plotted as dotted curves, was obtained from elastic scattering data analysis at $E_{\text{c.m.}}=32.8$ MeV [10].

$$\Delta\mathcal{V}=P\mathcal{V}^{\pi}p\frac{1}{E+i\epsilon-p(H_0+\mathcal{V}^{\pi})p}p\mathcal{V}^{\pi}P. \qquad (3)$$

Even for few states in p, this is hard to evaluate because of coupling between all the p-space states. The potential $\mathcal{V}^{\pi}$ is the formal ''bare'' potential and $\Delta\mathcal{V}$ is the formal DPP.

III. ^{6}He+p ELASTIC SCATTERING

Elastic scattering of radioactive ^{6}He from protons was recently studied and DPPs for this system were found [9,10]. In Ref. [9], scattering data taken at a c.m. energy of 21.57 MeV were analyzed using the CDCC method, which included the effects of breakup processes. The DPP potential was extracted from these calculations using the weighted trivially equivalent (WTE) method as described by Thompson *et al.* [11]. The real part of this potential has general features found previously for other weakly bound projectiles [1,2]. The most conspicuous features are surface repulsion, attraction in the nuclear interior and general, but not radially uniform, absorption.

Lapoux *et al.* [10] studied ^{6}He+p elastic scattering at the higher c.m. energy of 32.8 MeV with an optical model analysis based on a folding potential derived from nucleon-nucleon interactions. They found that they could describe the data when a purely phenomenological DPP is added to the central folding model potential. However, this DPP, the dotted line in Fig. 1, is very different from the WTE DPP of Rusek *et al.* [9], the dashed line in Fig. 1. Imaginary parts of both DPPs have different signs and different strengths. The real parts at p-^{6}He separations larger than 2 fm are of the same repulsive character but the potential of Lapoux *et al.* [10] is much stronger. At separations smaller than 2 fm the difference between the two DPPs is even larger. The potential of Rusek *et al.* [9] becomes slightly attractive while the phenomenological potential becomes increasingly repulsive as r decreases. These discrepancies cannot be due to the different energies. The solid line in Fig. 1 represents the new DPP presented in this work and discussed below. The WTE potential of Rusek *et al.* does not represent the CDCC DPP accurately at small p-^{6}He separations, since one-channel calculations with this DPP added to the bare potential do not reproduce the results of the original CDCC calculations at backward scattering angles.

IV. MODEL ADOPTED FOR BREAKUP OF ^{6}He

In order to study the effect of ^{6}He breakup on low energy elastic scattering one needs a three-body model which can account for coupling to resonant and nonresonant states in the continuum. Unfortunately, such a model is not available yet. The model which can be used at present is a two-body coupled-channels model where the continuum of breakup states is discretized into energy bins with square-integrable wave functions.

In the model used by Rusek *et al.* [9] the ^{6}He nucleus was assumed to have a two-body $\alpha+2n$ cluster structure with the spin of the dineutron set to $s=0$. Breakup into continuum states with relative orbital angular momentum $L=0$, 1, 2, 3 was included by discretizing the continuum and there was coupling to the $L=2$ resonance at 1.8 MeV excitation energy. Coupling of multipolarities from $\Delta L=0$ to $\Delta L=3$ between the various channels was included. The choice of input parameters is described in Ref. [9], as are the details of how the continuum was discretized. Three different geometries of the potential binding the α core and dineutron into ^{6}He were used in Ref. [9]. Most of the calculations in the present work are based on set II parameters of that paper. We also present calculations involving the set I parameters in order to establish the sensitivity of the general results to such details.

Recent studies of ^{6}He breakup on various targets at an energy of 23.9 MeV/A led to the conclusion that the distribution of angle between the two neutrons shows a tendency towards the dineutron model [12]. In Ref. [9], the ^{1}H(^{6}He,α)^{3}H reaction was calculated using CCBA, so no representation of the contribution to the DPP of coupling to this or other reaction channels was included. All CDCC calculations were performed using computer code FRESCO [13].

V. INVERSION OF THE ELASTIC SCATTERING S MATRIX

A. Establishing the parameters for IP inversion

The iterative perturbative (IP) S-matrix to potential inversion procedure [1] is well developed and has been applied to a wide variety of cases. For details of recent developments

and earlier references, see Ref. [3] which presents test cases showing the precision achievable. The present calculations were performed using the IP inversion code IMAGO [14].

IP inversion requires a choice of the starting reference potential (SRP) and the inversion basis. The SRP is the starting point for the iterative inversion process and the inversion basis is the set of functions in which the correction to the SRP is expanded. Too large a basis can lead to a potential having spurious oscillations, although the use of SVD matrix methods moderates this [15]. In favorable cases the SRP does not need to be close to the unknown potential, and can be often be zero, but in general the SRP should be reasonably close to the potential which is sought. The natural choice of SRP when determining the DPP is the bare potential. The present case is quite unfavorable since the small number of active partial waves is not much greater than the number of parameters required to describe the potentials. This makes the choice of inversion basis somewhat critical and will be discussed elsewhere [16].

B. Test of the method; inverting S_{lj} for the one-channel case

The accuracy of the inversion procedure for ^{6}He scattering from protons at $E_{\mathrm{c.m.}}=21.57$ MeV was confirmed by inverting the S matrix for the case with the channel coupling switched off, one-channel calculations. The corresponding potential, the bare potential, is just the elastic channel input potential for the CDCC calculation. The inversion parameters were chosen so that the result is free of spurious oscillations and is stable to changes in SRP and inversion basis. The optimum potential representing the bare potential will be referred to as POT8. A full discussion of the determination of POT8, will be presented elsewhere [16], where we present an account of the necessary features of the inversion basis required for successful IP inversion in this regime. POT8 gave a good representation of the uncoupled S matrix, agreed with the bare potential of the CDCC calculations and was used as the SRP for subsequent inversions.

C. Inversion of the CDCC S matrix

The CDCC calculations included the breakup channels as specified in Sec. IV. The calculations were performed for two ^{6}He energies 151 and 245.4 MeV, corresponding to $E_{\mathrm{c.m.}}=21.57$ and 35.06 MeV, respectively. Potentials corresponding to the S-matrix elements from those calculations were found by IP inversion. The DPPs were calculated by subtracting POT8, rather than the CDCC bare potential, from the subsequent inverted potentials. Calculating the DPP as the difference between two potentials both derived by IMAGO makes any small disparities between IMAGO and the coupled channel code FRESCO irrelevant.

The various potentials can usefully be quantified in terms of their low order moments. These are well determined phenomenologically for light ions, and also subject to useful folding model relations [17]. They are the volume integrals per nucleon pair J and root mean square radius r_{rms} defined as

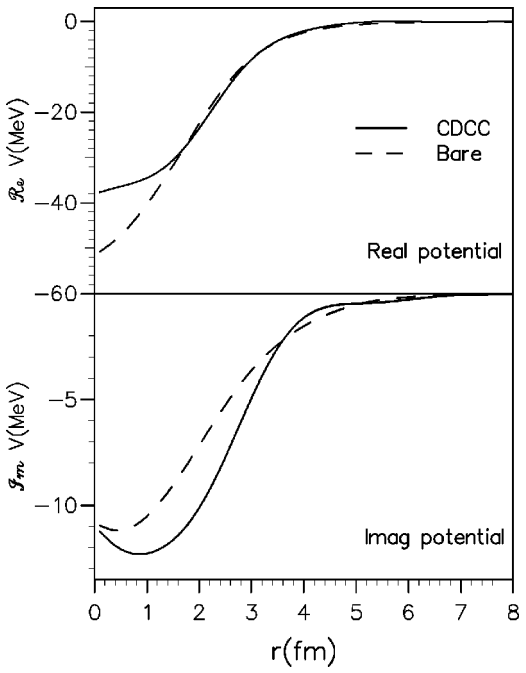

FIG. 2. For $E_{\mathrm{c.m.}}=21.57$ MeV, the dashed line represents POT8, the central bare potential as determined by inverting S_{lj} for the one channel calculation. The solid line represents the corresponding potential for the full CDCC calculation labeled IP(1), set II, in Tables I and II.

$$J=\frac{4\pi}{N_{\mathrm{P}}N_{\mathrm{T}}}\int_0^\infty V(r)r^2dr \tag{4}$$

and

$$(r_{\mathrm{rms}})^2=\langle r^2\rangle=\frac{4\pi}{N_{\mathrm{P}}N_{\mathrm{T}}J}\int_0^\infty V(r)r^4dr, \tag{5}$$

where N_{P} and N_{T} are the numbers of projectile and target nucleons.

The CDCC inverted central potentials leading to the DPPs shown as solid lines in Fig. 1 are shown in Fig. 2. They can be considered well established down to 0.5 fm. All four components of the DPPs are presented in Fig. 3. For both energies, the central real part is substantially repulsive at the nuclear center and has a repulsive surface tail, but is attractive for $1.5\leqslant r\leqslant 3$ fm. The central imaginary part is predominantly absorptive but has emissive regions, a general feature of DPPs and related to the fact that they are a local representation of a nonlocal term [4].

The volume integrals of the central potentials, bare (1 channel) and CDCC labeled IP(1), are presented in lines 1, 2, 9, and 10 of Table I. The changes in these, given as absolute and percentage, reflect the overall repulsive plus absorptive effect of the breakup. The change in the real r_{rms} is also of interest, and is relevant to the extraction of nuclear sizes from elastic scattering; it is presented in Table II. Breakup evidently has the effect of making the nucleus look smaller. Nuclei would, on this account, be larger than analyses of experiments using simple folding models might suggest.

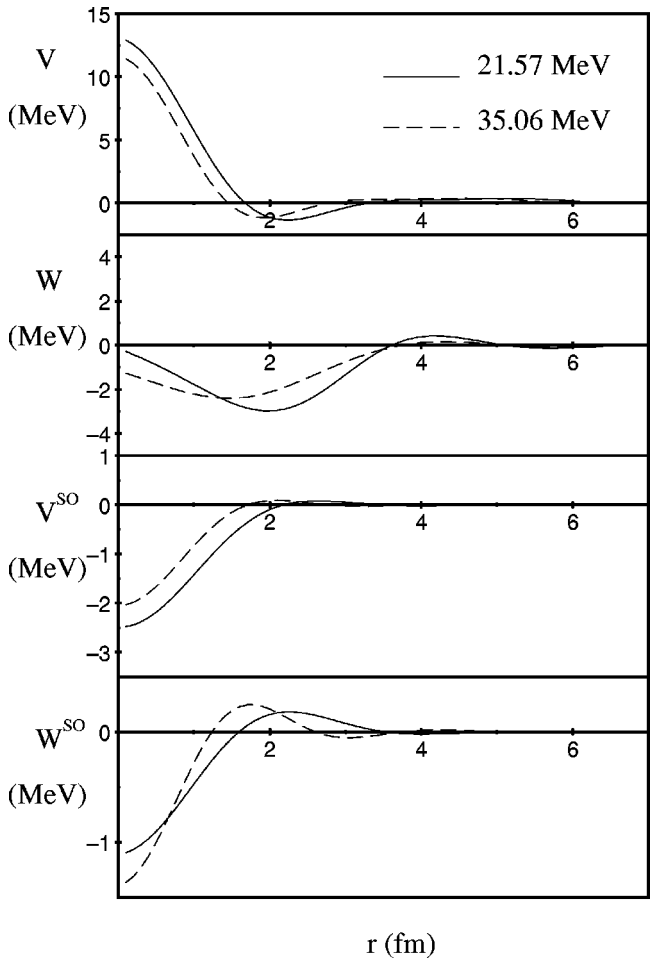

FIG. 3. Real and imaginary central (top) and the real and imaginary spin-orbit components of the DPP for ^{6}He+p. The solid and dashed lines correspond $E_{\text{c.m.}}=21.57$ and 35.06 MeV, respectively.

The real and imaginary parts of the DPP at 35.06 MeV are remarkably similar to those found at 21.57 MeV, as can be seen in Fig. 3. The change in the DPP with energy can be seen quantitatively by comparing the corresponding volume integrals and rms radii presented in lines 1 and 2 and lines 9 and 10 in Tables I and II. Apart from the change in ΔJ_R, the dynamic polarization effect falls slightly with increasing energy, as expected. The decrease is probably too small to be of phenomenological significance since the energy dependence of J_R is largely due to knock-on exchange.

As a check, the inverted potentials were input into FRESCO to verify that they reproduced the CDCC calculations to high accuracy, consistent with small differences between IMAGO and FRESCO, see Ref. [16]. The agreement between the full CDCC differential cross-section and that calculated without channel coupling using the sum of the bare potential and the DPP is shown in Fig. 4 where the angular distributions are barely distinguishable. This figure also shows that the agreement with the data of Refs. [18,19] is very good forward of 60°. We also see from Fig. 4 that the role of the spin-orbit term increases with energy. One-channel calculations using the inverted DPP with this term omitted are plotted as dot-dashed lines. At the higher energy the spin-orbit term significantly enhances the differential cross section at backward angles.

D. Alternative inversion

The 21.57 MeV CDCC inversion was repeated without forcing the inversion to such a close fit to the CDCC S matrix. This leads to potentials which are somewhat smoother in the surface region. The results are labeled IP(2) in lines 13 and 14 of Tables I and II. The new inversion provides a better comparison with later cases for which inversion was carried out in a similar way. The volume integrals are close to those in lines 1 and 2 of Table I. The rms radii in lines 13

TABLE I. Volume integral per nucleon pair J (MeV fm^3) of the ^{6}He+p effective bare+DPP potentials representing the one-channel and CDCC calculations. The ΔL column lists the allowed multipolarities of the couplings while ΔJ represents the change of J and ΔJ % is the percentage change. Sets I and II correspond to alternative potentials binding α and dineutron into ^{6}He as specified in Table I of Ref. [9]. Lines are numbered to facilitate reference from the text.

	J	$E_{\text{c.m.}}$	Set	1 chan	CDCC	ΔL	ΔJ	ΔJ %
1	IP(1), Real	21.57 MeV	II	559.34	526.20	0,1,2,3	−33.14	−6.0
2	IP(1), Imaginary	21.57 MeV	II	252.24	298.31	0,1,2,3	46.07	18.3
3	Real	21.57 MeV	II	559.34	527.39	0,1,2	−31.95	−5.71
4	Real	21.57 MeV	II	559.34	554.14	0,1	−5.2	−0.93
5	Real	21.57 MeV	II	559.34	558.00	0	−1.34	−0.24
6	Imaginary	21.57 MeV	II	252.24	298.89	0,1,2	46.65	18.49
7	Imaginary	21.57 MeV	II	252.24	251.43	0,1	−0.81	−0.32
8	Imaginary	21.57 MeV	II	252.24	262.62	0	10.38	4.11
9	Real	35.06 MeV	II	559.37	524.71	0,1,2,3	−34.66	−6.2
10	Imaginary	35.06 MeV	II	252.31	288.36	0,1,2,3	36.05	14.3
11	Real	21.57 MeV	I	559.34	513.90	0,1,2,3	−45.44	−8.12
12	Imaginary	21.57 MeV	I	252.24	313.06	0,1,2,3	60.82	24.11
13	IP(2), Real	21.57 MeV	II	559.34	525.28	0,1,2,3	−33.96	−6.07
14	IP(2), Imaginary	21.57 MeV	II	252.24	297.82	0,1,2,3	45.58	18.07

TABLE II. Root mean square radius $r_{\rm rms}$ (fm) of the ^{6}He$+p$ effective bare+DPP potentials representing the one-channel and CDCC calculations. The ΔL column lists the allowed multipolarities of the couplings while K is their sum. $\Delta r_{\rm rms}$ represents the change in $r_{\rm rms}$ and $\Delta r_{\rm rms}$ % is the percentage change. Sets I and II correspond to different potentials binding α and dineutron into ^{6}He and listed in Table I of Ref. [9].

	$r_{\rm rms}$	$E_{\rm c.m.}$	Set	1 chan	CDCC	ΔL	K	$\Delta r_{\rm rms}$	$\Delta r_{\rm rms}$ %
1	IP(1), Real	21.57 MeV	II	3.098	2.911	0,1,2,3	6	−0.187	−6.0
2	IP(1), Imaginary	21.57 MeV	II	3.741	3.614	0,1,2,3	6	−0.127	−3.4
3	Real	21.57 MeV	II	3.098	2.927	0,1,2	3	−0.171	−5.52
4	Real	21.57 MeV	II	3.098	3.006	0,1	1	−0.092	−2.97
5	Real	21.57 MeV	II	3.098	3.098	0	0	0.0	0.0
6	Imaginary	21.57 MeV	II	3.741	3.633	0,1,2	3	−0.108	−2.89
7	Imaginary	21.57 MeV	II	3.741	3.736	0,1	1	−0.005	−0.134
8	Imaginary	21.57 MeV	II	3.741	3.692	0	0	−0.049	−1.31
9	Real	35.06 MeV	II	3.097	2.939	0,1,2,3	6	−0.158	−5.1
10	Imaginary	35.06 MeV	II	3.745	3.635	0,1,2,3	6	−0.110	−2.9
11	Real	21.57 MeV	I	3.098	3.058	0,1,2,3	6	−0.040	−1.29
12	Imaginary	21.57 MeV	I	3.741	3.877	0,1,2,3	6	0.136	3.64
13	IP(2), Real	21.57 MeV	II	3.098	2.885	0,1,2,3	6	−0.213	−6.88
14	IP(2), Imaginary	21.57 MeV	II	3.741	3.626	0,1,2,3	6	−0.115	3.07

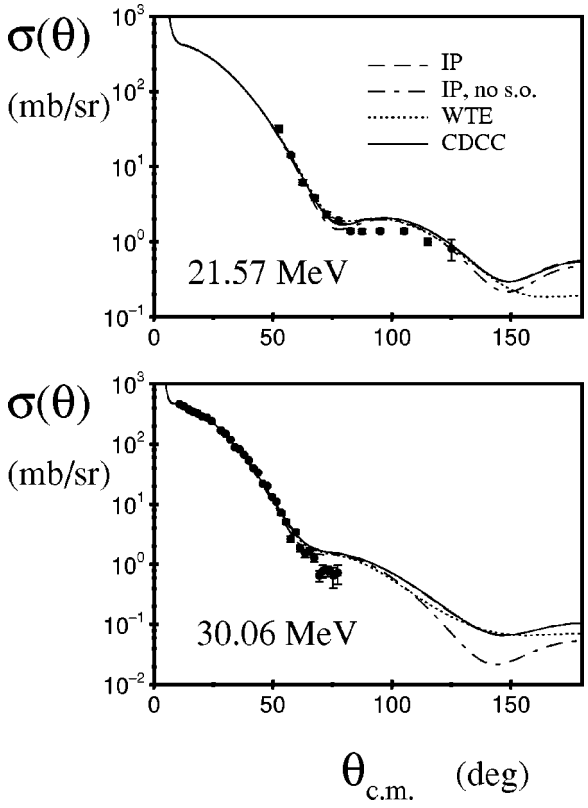

FIG. 4. Angular distributions of the differential cross section for elastic scattering of ^{6}He from p. Data sets are from Refs. [18,19]. Solid curves show results of CDCC calculations of Ref. [9]. The other curves correspond to the one-channel calculations with the effective potential consisted of the bare plus DPP potentials. Results of the one-channel calculation with the DPP obtained by means of IP method (dashed curves) are practically indistinguishable from the full CDCC results. Dot-dashed curves show results of one-channel calculation with DPP obtained in this work but without spin-orbit term.

and 14 of Table II differ a little more, but rms radii are more sensitive than volume integrals since the former involve radial integrals involving a higher power of r. The far surface is also susceptible to the presence of noise in S_{lj}. The four components of the resulting DPPs are compared in Fig. 5, where the solid lines represent the original DPP, and the dotted lines the DPP obtained as described here.

The alternative inversions indicate the reliability of the inversion method. The true DPP is nonlocal and l-dependent resulting in some "waviness" in the local and l-independent potential found by inversion. The inevitable noise in the S-matrix elements contributes to this. Restricting the precision to which S_{lj} is fitted ensures that the waviness in the solution is not a fit to numerical noise in S_{lj}. This flexibility is specific to IP inversion.

E. Alternative ^{6}He binding interaction

It has recently become evident that CDCC calculations with the set I parameters of the α+dineutron binding potential from Ref. [9] appear to give a better description of inelastic scattering data than calculations with set II parameters. We therefore compare the DPP generated with set I parameters with that from set II, see Fig. 5, and lines 11 and 12 of Tables I and II.

Set I parameters lead to much greater repulsion in the real potential and greater absorption in the imaginary potential as measured by ΔJ_1. This is consistent with the greater $B(E2)$ and inelastic scattering cross section to the 2^+ state. Interestingly, the effect on the rms radius was small in the real part (line 11 of Table II) and of reverse sign in the imaginary part (line 12) compared to what is given in lines 1 and 2, or alternatively, lines 13 and 14. This might be connected with the fact that the geometric parameters in the set I and set II parameters were different.

The rms radii of the real parts of the CDCC potentials, lines 1, 11, and 13 of Table II, are somewhat higher than

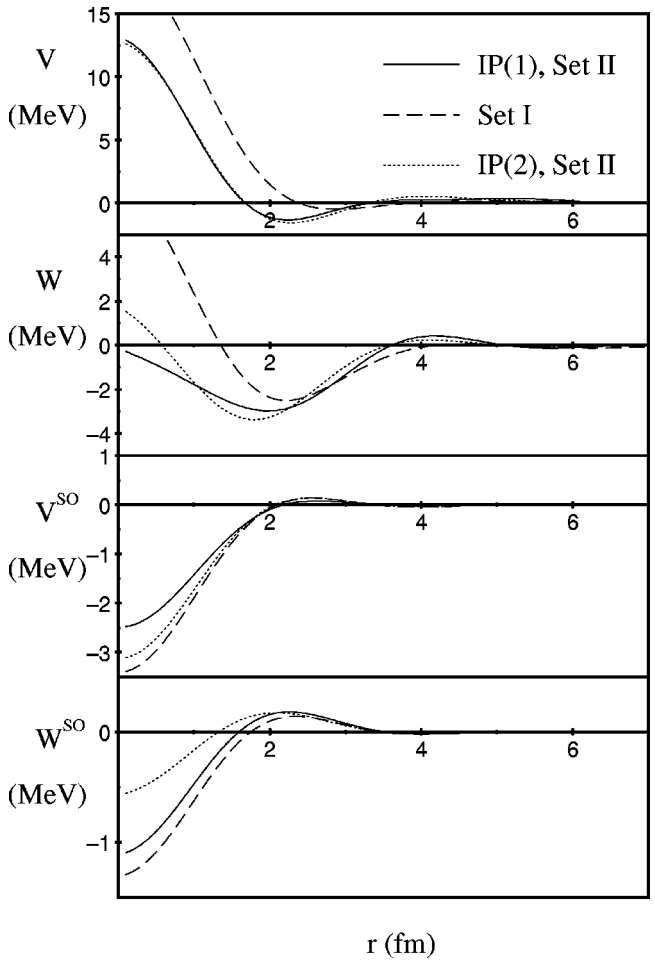

FIG. 5. For 21.57 MeV c.m. energy comparing components of DPP found with different α+dineutron binding potentials; solid lines correspond to set II, dashed lines correspond to set I. Dotted lines show DPP found from an alternative inversion, see text for details.

expected. However, they correspond to reasonable fits to the angular distributions, especially with set I parameters for which the CDCC inverted potential has a greater rms radius than for set II.

VI. PROPERTIES OF DYNAMIC POLARIZATION POTENTIALS

A. Comparison with other DPPs

In Ref. [9], the polarization potential for ^{6}He+p at $E_{\text{c.m.}}=21.57$ MeV was extracted from the CDCC calculations using the WTE method described by Thompson *et al.* [11]. Trivially equivalent L-dependent polarization potentials were weighted according to the partial wave reaction cross sections. It is of interest to compare the exact local DPP calculated by means of IP method with the approximate WTE DPP. The real and imaginary parts of the central polarization potentials obtained from inversion and by means of approximate WTE method are compared in Fig. 1. The agreement is only qualitative. The difference in the real part at small radii is dramatic, and we have verified that the scattering, in this case, is sensitive to the potential for $r<2$ fm.

The DPP as found by inversion and the WTE approximate DPP can be compared by checking how well they reproduce the CDCC observables when added to the one-channel potential. As shown in Fig. 4, the inversion DPP gives virtually perfect agreement, but the WTE fails at backward angles. Dashed lines representing one-channel calculations with the effective potential being the sum of bare potential and IP DPP are hardly to be distinguished from the solid lines representing the CDCC calculations. (The small discrepancy is due to small differences between IMAGO and FRESCO parameters, see Ref. [16].) Calculations with the WTE DPP are represented by the dotted lines which are distinct from the solid lines from 50° outwards.

In their analysis of ^{6}He+p elastic scattering data at $E_{\text{c.m.}}=32.8$ MeV, Lapoux *et al.* [10] introduced a phenomenological DPP with a repulsive real part.

$$U_{\text{pol}}=-(V_{\text{pot}}+\text{i}W_{\text{pot}})\exp(r/a_{\text{pot}})/[1+\exp(r/a_{\text{pot}})]^2, \quad (6)$$

where $V_{\text{pot}}=-47.2$ MeV, $W_{\text{pot}}=-4.4$ MeV, and $a_{\text{pot}}=1.33$ fm. The real part is repulsive at all radii, about 12 MeV at the origin, falling to about 2 MeV at 4 fm (Fig. 1). It agrees quite well with the set II CDCC-inversion potential near the nuclear center and in the nuclear surface, but has the opposite sign between 1.5 and 3 fm, an important radial range.

The disagreement of the imaginary parts is more serious, that of Ref. [10] being wholly emissive in sign. While DPPs found by inversion can be emissive over a limited radial range, as a consequence of underlying nonlocality, a wholly emissive DPP is implausible, and, in fact, contrary to what is found by inversion. It also contradicts general properties of breakup DPPs as found in other cases [1,2] and it is most unlikely that the various omitted reaction channels would generate overall emission. The extraction of a DPP by this means hinges on the use of the folding model. We take the interesting result of Ref. [10] to be evidence of the limits of the folding model. The target nucleus is very different from those for which the folding model was established so it is not surprising that it fails to predict the small imaginary part.

Determining the DPP by fitting an additive term is preferable to the common practice of applying uniform multiplicative factors to the real and imaginary parts. Folding models based on a local density model present the radial shape and magnitude of a potential as a single consistent package. Such a model cannot fully represent phenomena connected with the density gradient in the nuclear surface. Probably the best way to determine the DPP phenomenologically is to fit an additive component to the folding model potential model independently. If the folding model is sound, this should reveal generic features that can be related to DPPs found by inversion. Unfortunately, establishing an unambiguous potential by model independent fitting requires elastic scattering data of much greater information content than is generally available, especially for unstable nuclei.

It has been shown [1,2] that the DPP arising from breakup processes has general features which apply to both deuterons and ^{6}Li projectiles scattering from nuclei ranging from carbon to tin. Similar conclusions have been found by Sakuragi [20] for the surface region using approximate inversion

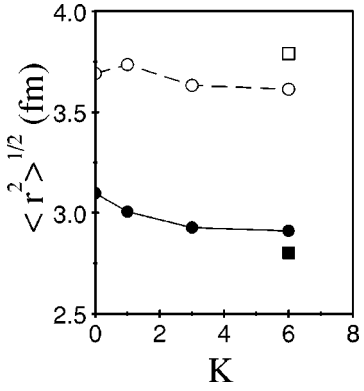

FIG. 6. Dependence of the root mean square radius of the central ^{6}He$+p$ potential on the multipolarities ΔL of the couplings included in the CDCC calculations. Number K is a sum of multipolarities, as shown in Table III. Full and open symbols correspond to the real and imaginary parts of the central potential, respectively. Dots represent the full calculations while the squares show results of the calculations without couplings between excited states included. The calculations were performed for 21.57 c.m. energy.

methods. However, for ^{6}He$+p$ the DPP is important down to $r \sim 0$, as generally true for proton-nucleus scattering. The most conspicuous general features of breakup on heavier nuclei are surface repulsion, attraction in the nuclear interior following a distinctive pattern, and general but not radially uniform absorption. General semiclassical arguments can be made explaining some of these features, but a full explanation is lacking. It is natural to ask whether the DPP for scattering from protons follows these trends. The real DPPs shown in Fig. 3 share with d or ^{6}Li breakup on heavier target nuclei the properties of repulsion in the surface ($r > 3.5$ fm) and increased absorption, but the behavior is different elsewhere. This might relate to the fact that the nuclear center has a different significance for more absorptive systems [2]. Similar comments apply to the imaginary parts.

B. Contribution of different multipolarities

A study of ^{6}He breakup performed by Wang *et al.* [12] has shown that for heavy targets this process is dominated by Coulomb $E1$ excitation while for light targets like Al or C the nuclear transitions are much more important. In the latter case other multipolarities than $\Delta L = 1$ may play an important role. It is straightforward to study the contribution to the DPP of channel couplings with different multipolarities. Since there are no spin-flip transitions included, the multipolarities ΔL of the breakup coupling interaction correspond to the states with the spin I that are directly coupled to the ground state. However, restricting the possible multipolarities does not in general restrict the coupling to that between the ground state and specific continuum states, but may permit various continuum-continuum couplings depending on what multipolarities are included. For example, if $\Delta L = 0$ is among the multipolarities included, then there is coupling between all continuum states of the same spin and parity.

Three CDCC calculations at $E_{\text{c.m.}} = 21.57$ MeV included all couplings with, respectively, multipolarities (i) $\Delta L = 0$,

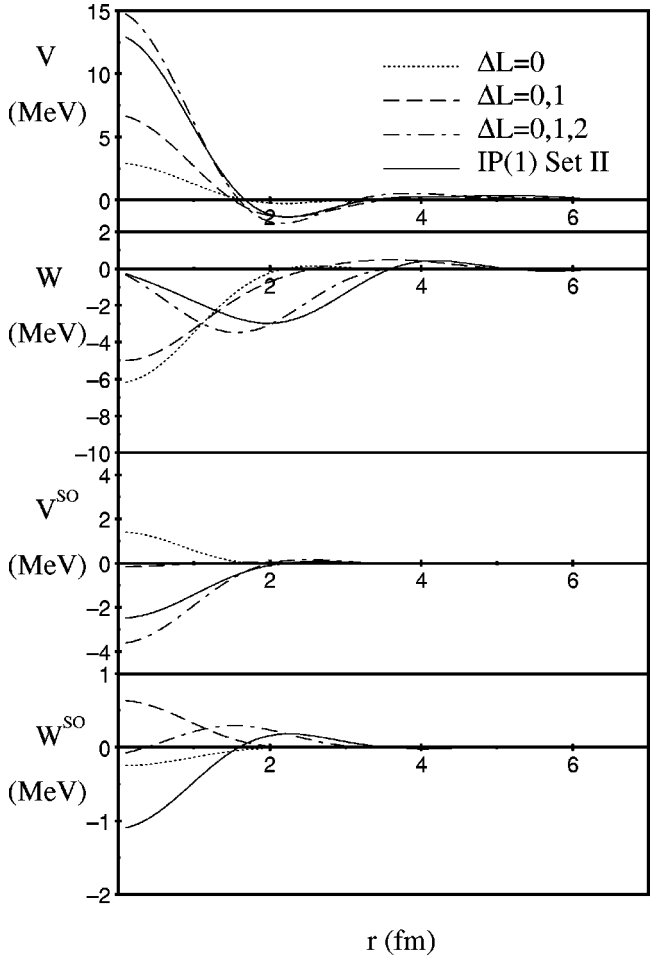

FIG. 7. Contributions of different multipolarities to DPP for 21.57 MeV c.m. energy

(ii) $\Delta L = 0$ and 1, and (iii) $\Delta L = 0$, 1, and 2. These three cases led to DPPs with central components characterized by the volume integrals given in lines 3 to 5 (real) and 6 to 8 (imaginary) in Table I. The corresponding changes in the rms radii are given in lines 3 to 5 and lines 6 to 8 in Table II. The dependence of the rms radii on the multipolarities included is plotted in Fig. 6 which shows how the radial sizes of the real and imaginary parts of the effective ^{6}He$+p$ potential are modified by coupling to breakup states.

It can be seen (Fig. 7) that when included alone, the monopole, $\Delta L = 0$, couplings make a relatively small contribution to the DPP; this restriction effectively excludes any but the $I = 0$ continuum states. The effect on the real potential is not a surface effect at all, but a small repulsion near the nuclear center with little change beyond 2 fm. The contribution of the dipole, $\Delta L = 1$, transitions are also quite small, and even somewhat paradoxical, since the overall effect on the volume integral of the imaginary potential is emissive (generative). The imaginary DPP with both monopole and dipole coupling is not uniformly emissive, however, being absorptive for $r < 2.5$ fm, emissive for $2.5 < r < 4$ fm, and absorptive in the far surface. This pattern closely follows the change in $|S_l|$ which is increased by the coupling for partial waves near $l = 3$. Quadrupole coupling has a large effect, contributing most of that seen in the complete calcu-

TABLE III. Volume integral per nucleon pair J (MeV fm^3) of the ^{6}He+p effective bare+DPP potentials representing the one-channel and CDCC calculations at $E_{\text{c.m.}}=21.57$ MeV. I^π is the spin of the excited states included in the CDCC calculations while ΔJ represents the change of J and ΔJ % is the percentage change. In the fourth column, cont.-cont. indicates whether the coupling between excited states was included.

	J	1 chan	CDCC	cont.-cont.	I^π	ΔJ	ΔJ %
1	Real	559.34	529.81	no	2^+	−29.53	−5.28
2	Real	559.34	529.52	no	$0^+,1^-,3^-$	−29.82	−5.33
3	Real	559.34	498.97	no	$0^+, 1^-, 2^+, 3^-$	−60.37	−12.1
4	Imaginary	252.24	306.85	no	2^+	54.61	21.65
5	Imaginary	252.24	252.87	no	$0^+, 1^-, 3^-$	0.53	0.21
6	Imaginary	252.24	306.42	no	$0^+, 1^-, 2^+, 3^-$	54.18	21.5
7	Real	559.34	530.71	yes	2^+	−28.63	−5.12
8	Real	559.34	557.83	yes	$0^+, 1^-, 3^-$	−1.51	−0.27
9	Imaginary	252.24	301.77	yes	2^+	49.53	19.64
10	Imaginary	252.24	258.97	yes	$0^+, 1^-, 3^-$	6.73	2.67

lations. Octupole coupling in the complete calculations appears to have a slightly emissive effect, as can be deduced from Table I.

Many other combinations of multipolarities could be studied. For example, the comparison of $\Delta L=2$ alone with $\Delta L=0, 2$ would give insight into the contribution of continuum-continuum coupling, but these effects are studied more directly in the next section.

C. Contribution of continuum-continuum coupling

The total contribution when many excited states are coupled includes the effect of the coupling between those states. When the coupling between excited states is included, the effect of particular states is not additive in a simple way. It is of interest to evaluate the effect of the coupling between excited states since this can throw light on just how various kinds of excitation processes contribute to the DPP. It is also salutary to see how large these effects are because the omission of these couplings greatly simplifies the calculation, and it is therefore tempting to omit them. Various calculations of the imaginary part of optical potentials, such as those of Coulter and Satchler [8], make that simplifying assumption; Green function methods present a very difficult iterative problem without it [7].

Feshbach theory [4] implies that when there is no coupling between excited states, the nonlocal (and l dependent) DPPs arising from the coupling to individual excited states add linearly. That is, the sum of the DPPs generated by coupling individual states to the ground state is just the overall nonlocal DPP when the states are simultaneously coupled to the ground state. It is expected that the local-equivalent potentials, as determined by inversion, should also add linearly. This can easily be tested and is what we have done.

Three calculations were performed, each with no coupling between excited states: one with all $\Delta L=2$ transitions from the ground state, one with all $\Delta L=0, 1, 3$ transitions, and one with all transitions. The results are presented in lines 1 to 6 in Tables III and IV. In effect, these are calculations including either the $I=2$ excited states or the $I=0, 1, 3$ excited states, respectively. They are *not* the same as full CDCC calculations omitting, respectively, $I=0, 1, 3$ excited states and $I=2$ excited states.

TABLE IV. Root mean square radius, r_{rms}, (fm), of the ^{6}He+p effective bare+DPP potentials representing the one-channel and CDCC calculations at $E_{\text{c.m.}}=21.57$ MeV. I^π is the spin of the excited states included in the CDCC calculations while Δr_{rms} represents the change of r_{rms} and Δr_{rms} % is the percentage change. In the fourth column, cont.-cont. indicates whether the coupling between excited states was included.

	r_{rms}	1 chan	CDCC	cont.-cont.	I^π	Δr_{rms}	Δr_{rms} %
1	Real	3.098	2.969	no	2^+	−0.129	−4.16
2	Real	3.098	2.962	no	$0^+, 1^-, 3^-$	−0.136	−4.39
3	Real	3.098	2.802	no	$0^+, 1^-, 2^+, 3^-$	−0.296	−9.6
4	Imaginary	3.741	3.710	no	2^+	−0.129	−4.16
5	Imaginary	3.741	3.844	no	$0^+, 1^-, 3^-$	−0.136	−4.39
6	Imaginary	3.741	3.790	no	$0^+, 1^-, 2^+, 3^-$	−0.296	−9.60
7	Real	3.098	2.983	yes	2^+	−0.115	−3.71
8	Real	3.098	2.973	yes	$0^+, 1^-, 3^-$	−0.125	−4.03
9	Imaginary	3.741	3.644	yes	2^+	−0.97	−2.592
10	Imaginary	3.741	3.731	yes	$0^+, 1^-, 3^-$	−0.010	−0.27

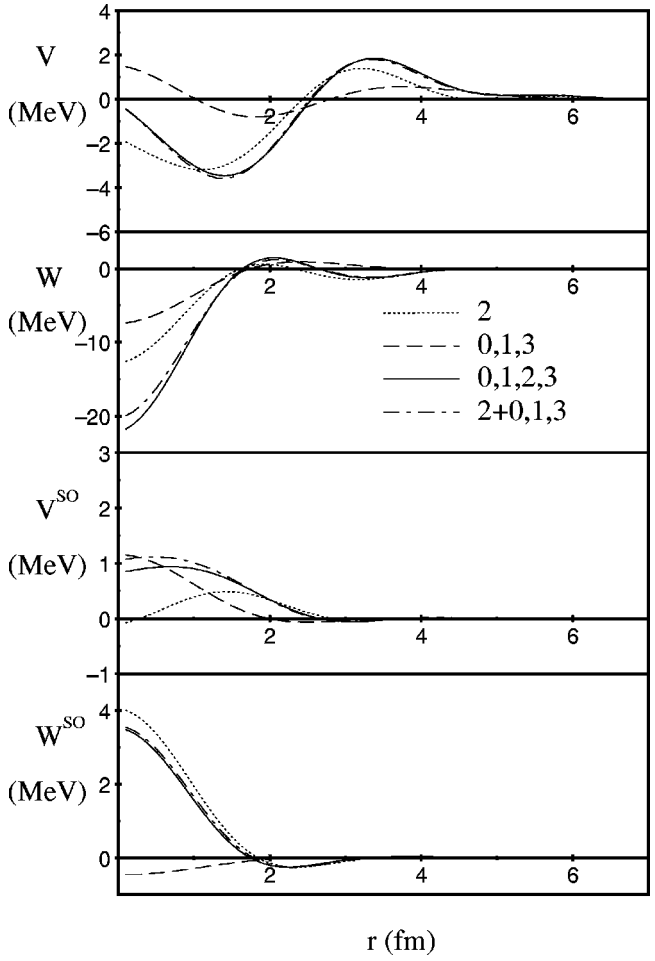

FIG. 8. Additivity of the potentials calculated with the continuum-continuum coupling omitted. Dotted lines show results with $I=2$ states included, dashed with $I=0,1,3$ excited states while the dash-dotted present their sum. Solid lines show results with all the states included.

The additivity that is expected when continuum-continuum coupling is omitted can be tested through the additivity of the volume integrals, as presented in Table III. The sum of the $I=2$ (line 1) and $I=0$, 1, 3 (line 2) real terms is -59.35 which is close to -60.37 (line 3); the corresponding values for the imaginary terms are 55.14 and 54.18 (lines 4, 5, and 6). The potentials also add point by point, as can be seen in Fig. 8. The addition is nearly perfect, the only exception being for the small real spin-orbit DPP near $r=0$. This confirms the additivity of the potentials for the L-independent local equivalents of the DPP as determined by inversion, and implies that IP inversion yields reliable detailed radial forms of the potential.

The corresponding changes in the rms radii are given in lines 1 to 6 in Table IV; there is no requirement for changes in the rms radii to add exactly, though they do approximately. By comparing lines 3 and 6 of Tables III and IV with the 21.57 MeV results in lines 13 and 14 of Tables I and II, we see that continuum-continuum coupling substantially reduces the DPP, particularly its real component. This effect is also shown in Fig. 6.

To evaluate the contribution of the coupling between excited states, we studied cases involving the same two sets of states: (i) including all excited states except those with $I=2$ and (ii) including $I=2$ excited states only. In both cases, all coupling between the included excited states was switched on. The resulting volume integrals and rms radii are presented in lines 7 to 10 in Tables III and IV. The contributions no longer add: compare $-28.63-1.51=-30.14$ with -33.96 of Table I and $49.53+6.73=56.26$ with 45.58 of Table I. Roughly speaking, the full CDCC repulsion is greater than the sum of its parts, but the full CDCC absorption is less than the sum of its parts.

The effect of coupling between excited state channels is greater than the change in the volume integrals suggests. Comparison of the DPPs plotted in Figs. 8 and 3 shows that continuum-continuum coupling completely changes the radial form. We conclude that calculations of the DPP must include coupling between excited state channels.

The CDCC potentials should, in principle, be adjusted to the particular set of channels coupled together so that different potentials should be used in calculations with $I=2$ only, $I=0$, 1, 3, etc. There is at present no practical way of establishing appropriate potentials.

VII. SUMMARY AND CONCLUSIONS

We have presented the DPP for breakup of ^{6}He on protons according to a specific model of ^{6}He described in Ref. [9]. There is considerable agreement between the radial form and the magnitude of the DPP at $E_{\mathrm{c.m.}}=21.57$ and 35.06 MeV. The radial shape of the real part is nonuniform, being repulsive in the surface and at the nuclear center, but attractive in the intermediate range. The imaginary part is absorptive overall, but is emissive near the surface, probably because it is a local equivalent to a nonlocal potential.

We find a consistent pattern in the way dynamic processes change the rms radius of the nuclear potential. This is significant when relating nuclear size to elastic scattering data.

It has not been possible in this case to evaluate the DPP due to stripping and pickup processes. These can be large, but rigorous evaluation is difficult because of nonorthogonality terms and complexities arising from antisymmetrization. Exchange processes and the associated nonlocalities make a full understanding of these reactions very challenging.

One conclusion is independent of further developments: the DPP cannot be represented by a uniform renormalization of a folding model potential. The folding model is valid as a guide to the depth of the potential in the surface using fits to forward angle data. Any requirement to renormalize a folding model potential reveals that the folding model is inadequate. This is not contradicted by the fact that angular distributions of limited angular range can be fitted reasonably well with such renormalization.

We have also shown that the IP method yields reliable potentials from CDCC S-matrix elements at quite low c.m. energies, and would probably work well at even lower energies as long as due care is taken to establish an appropriate inversion basis. It is the only inversion method capable of yielding reliable central and spin-orbit potentials down to

radii $r \sim 0$, particularly when the set of S_{lj} contains the inevitable numerical ''noise'' associated with coupled channel calculations. We have indicated the extent to which the radial shape and other characteristics are well determined. A necessary (though not sufficient) condition for the point by point additivity of the potentials of Fig. 7 is the reliable determination of the radial form of the potentials by inversion.

In the course of this work, we have shown that the standard WTE method yields an inadequate representation of the DPP in the case of proton scattering, for which the DPP at small r is important. When the formal DPP is both highly L dependent and relevant for r less than surface values, the nature of the partial wave weighting is crucial. The inversion method, in giving a DPP which precisely fits elastic scattering, yields a local potential that can be compared with potentials found by means of precision local-potential phenomenology. Inversion can readily evaluate any specific application of the WTE method.

We pointed out in Sec. VI A that the DPP for $p+^6$He did not conform closely to the generic properties of the DPP for breakup of deuterons or ^{6}Li on heavier nuclei. Understanding the generic properties of the DPP and how exceptions occur is an important part of understanding nucleus-nucleus elastic scattering. Many features of the DPP are unexplained, and, to provide clues, future work should explore, for a range of cases, the way the DPP depends upon the L-transfer, Q value, and the bare potential, the complex coupling potentials, etc. The present work establishes the feasibility of using IP inversion together with coupled channel calculations as a tool for such studies.

ACKNOWLEDGMENTS

R.S.M. thanks N. Alamanos and V. Lapoux for enlightening discussions.

[1] R.S. Mackintosh and A.M. Kobos, Phys. Lett. **116B**, 95 (1982).
[2] A.A. Ioannides and R.S. Mackintosh, Phys. Lett. **169B**, 113 (1986).
[3] S.G. Cooper, V.I. Kukulin, R.S. Mackintosh, and V.N. Pomerantsev, Nucl. Phys. **A677**, 187 (2000).
[4] H. Feshbach, Ann. Phys. (N.Y.) **5**, 357 (1958); **19**, 287 (1962).
[5] S.G. Cooper, R.S. Mackintosh, and A.A. Ioannides, Nucl. Phys. **A472**, 101 (1987).
[6] D.T Khoa, G.R. Satchler, and W. von Oertzen, Phys. Rev. **51**, 2069 (1995).
[7] R.S. Mackintosh, Nucl. Phys. **A164**, 398 (1971).
[8] C.A. Coulter and G.R. Satchler, Nucl. Phys. **A293**, 269 (1977).
[9] K. Rusek, K.W. Kemper, and R. Wolski, Phys. Rev. C **64**, 044602 (2001).
[10] V. Lapoux, N. Alamanos, F. Auger, Y. Blumenfeld, J-M. Casandjian, M. Chartier, M.D. Cortina-Gil, V. Fékou-Youmbi, A. Gillibert, J.H. Kelley, K.W. Kemper, M. MacCormick, F. Maréchal, F. Marie, W. Mittig, F. de Oliviera Santos, N.A. Orr, A. Ostrowski, S. Ottini-Hustache, P. Roussel-Chomaz, J-A. Scarpaci, J-L Sida, T. Suomijärvi, and J.S. Winfield, Phys. Lett. B **517**, 18 (2001).
[11] I.J. Thompson, M.A. Nagarajan, J.S. Lilley, and M.J. Smithson, Nucl. Phys. **A505**, 84 (1989).
[12] J. Wang, A. Galonsky, J.J. Kruse, E. Tryggestadt, R.H. White-Stevens, P.D. Zecher, Y. Iwata, K. Ieki, A. Horvath, F. Deak, A. Kiss, Z. Seres, J.J. Kolata, J. von Schwarzenberg, R.E. Warner, and H. Schelin, Phys. Rev. C **65**, 034306 (2002).
[13] I.J. Thompson, Comput. Phys. Rep. **7**, 167 (1988).
[14] S.G. Cooper, program IMAGO (unpublished).
[15] S.G. Cooper and R.S. Mackintosh, Nucl. Phys. **A513**, 373 (1990).
[16] R.S. Mackintosh (in preparation).
[17] G.R. Satchler, *Direct Nuclear Reactions* (Clarendon Press, Oxford, 1983).
[18] R. Wolski, A.S. Fomichev, A.M. Rodin, S.I. Sidorchuk, S.V. Stepantsov, G.M. Ter-Akopian, M.L. Chelnokov, V.A. Gorshkov, A.Yu. Lavrentev, Yu.Ts. Oganessian, P. Roussel-Chomaz, W. Mittig, and I. David, Phys. Lett. B **467**, 8 (1999).
[19] A. de Vismes, P. Roussel-Chomaz, W. Mittig, A. Pakou, N. Alamanos, F. Auger, J.-C. Angélique, J. Barrette, A.V. Belozyorov, C. Borcea, W.N. Catford, M.-D. Cortina- Gil, Z. Dlouhy, A. Gillibert, V. Lapoux, A. Lepine-Szyly, S.M. Lukyanov, F. Marie, A. Musumarra, F. de Oliveira, N.A. Orr, S. Ottini-Hustache, Y.E. Penionzhkevich, F. Sarazin, H. Savajols, and N. Skobelev, Phys. Lett. B **505**, 18 (2001).
[20] Y. Sakuragi, Phys. Rev. C **35**, 2161 (1987).